Trends in Chemistry

CellPress
REVIEWS

Focus on Perovskite Materials

Review

Metal Ions in Halide Perovskite Materials and Devices

Peter N. Rudd[1] and Jinsong Huang[1,*]

The influence of metal ions on perovskite properties and resulting device performance has been undeniable in progressing the field of inorganic and organic–inorganic hybrid perovskites. Here we provide a review on the capacity of metal ions to impart a broad range of effects from controlling crystallization to the alloying, doping, and passivation of perovskite materials. Although some metal ions have already proved effective in modulating bandgaps through alloying, their ability to control crystallization, carrier concentration, and emissive effects still require significant improvements in fundamental understanding. This presents enormous opportunities in research that may afford novel properties and applications through unparalleled control of perovskite materials.

Highlights

Incorporation of metal ions in halide perovskites proves to be a modern tool for tuning material properties to afford novel solutions for enhanced efficiency and stability in perovskite electronic devices.

The unique properties of any given metal from the periodic table promises myriad opportunities to serve the application of perovskite materials in various electronic devices.

Capitalizing on chemical interactions between metal ions and perovskite structures has demonstrated the capacity to stabilize halide perovskite materials, a crucial step in the transition of perovskite solar cells from bench to market.

Current Status of Alloying and Doping in Perovskite Devices

Perovskite materials have emerged as a focal point in optoelectronic research, demonstrating exceptional intrinsic properties including long charge-carrier diffusion length, tunable bandgap, low **mid-gap trap density** (see Glossary), high absorption coefficient, and efficient photoluminescence (PL) [1–8]. The ability to harness all of these desired properties in one material coupled with the scalable, low-cost solution processability has made them highly attractive for next-generation electronic devices [9,10]. To date, perovskite materials have afforded detectors with excellent sensitivity and low noise for photons and X-rays, light-emitting diodes (LEDs) with internal quantum efficiencies approaching unity in the visible and near-IR regions, lasers with high quality factors resulting in an ultralow threshold (220 nJ cm^{-2}), and most notably perovskite solar cells (PVSCs) and perovskite–silicon tandem devices recently achieving certified efficiencies of 23.7% and 28.0%, respectively [10–16].

Such impressive performance has been made possible by the ABX_3 structure of perovskite materials, where A is a +1 cation that is typically either organic [methylammonium (MA) or formamidinium (FA)], inorganic [cesium (Cs^+)], or an organic–inorganic hybrid composition (OIHP), B is a metal cation most commonly comprising lead (Pb^{2+}), and X is a halide or mixture of halide anions (Cl^-, Br^-, or I^-). The ABX_3 structure of perovskites allows tremendous capabilities in compositional engineering to tune the physical properties of perovskite materials. Box 1 provides an overview of the mechanism and theory for tuning bandgap and mid-gap trap density. However, depending on the chosen composition, the material is capable of conforming to various crystal structures – cubic, tetragonal, orthorhombic, or hexagonal – with differing properties [17]. Box 2 explains further the ability to predict the phase and stability of a given composition.

Recent research on perovskite **defect passivation** and compositional engineering for improved solar-cell performance and stability has accelerated the field [18]. To realize novel optoelectronic properties for targeted commercial applications, it is necessary to further optimize and tune the photoelectric performance of halide perovskites. To address these needs and further improve device efficiency and stability, research has recently taken interest in the incorporation of metal ions

[1]Department of Applied Physical Sciences, The University of North Carolina at Chapel Hill, Chapel Hill, NC 27599, USA

*Correspondence:
jhuang@unc.edu (J. Huang).

Box 1. Predicting Perovskite Formation and Stability

First reported by Goldschmidt to describe the predicted structure of oxide perovskites, the Goldschmidt tolerance factor has been proven equally capable of providing a simple and reliable empirical index for predicting the structure and stability of both hybrid and inorganic perovskite materials. Using the following expression,

$$t = \frac{r_A + r_X}{\sqrt{2}\,(r_B + r_X)}, \quad [I]$$

the tolerance factor (t) is determined by the ionic radii of the A cation (r_A), the B cation (r_B), and the X anion (r_X). For compositions with a mixture of cations for A or B, or a mixture of halides for X, an effective ionic ratio is estimated by using the weighted average of the atomic ratio, as described by G. Kieslich and coworkers [94]. Although compositions with $0.71 < t > 1.0$ should all result in a perovskite phase, experimental results reveal that current perovskite materials are achieved when $0.85 < t > 1.0$. When considering the tolerance factor only, experimental perovskite materials have been found to be stable only when $0.9 < t > 1.0$. Due to significant tilt in the BX_6 octahedron, the structure is destabilized if $t < 0.9$ and the formation of a hexagonal phase occurs if $t > 1.0$.

Although the tolerance factor provides a simple screen of possible compositions, it is not capable of determining an accurate thermodynamic understanding of resulting stabilities. To more accurately describe stability, Li and colleagues were the first to use the octahedral factor (μ), which is equal to the ratio of r_B to r_X, in conjunction with the tolerance factor to produce a (t, μ) map capable of qualitatively displaying the threshold of perovskite stability [95,96]. A qualitative thermodynamic understanding of the prediction of stability was not thoroughly explored until Sun and Yin considered the decomposition energies (H_D) of materials (Figure I) [97]. It was also found that as a stability descriptor, $(\mu + t)^n$ where n is the atomic packing fraction provides a linear correlation to calculated H_D and the ability to predict the stability of perovskites with ~90% accuracy. Based on existing stable inorganic halide perovskites, stability can be achieved in the range $0.813 < t < 1.107$ and $0.377 < \mu < 0.895$ [97]. It should be noted that these works consider fully inorganic perovskites and that when an organic cation like MA or FA is introduced, it is difficult to provide predictions with such high accuracy due to the heterogeneous distribution of charge, nonspherical shape, and rotation within the lattice.

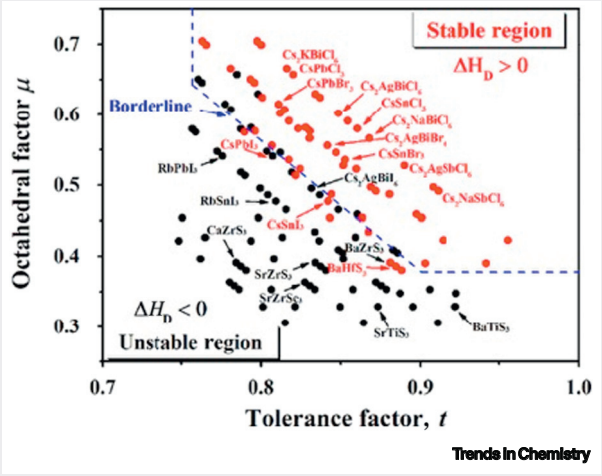

Figure I. Map of (t, μ) for a Number of Perovskite Compounds Where Those in Red Have $H_D > 0$ (predicting the structure to be stable) and those in black have $H_D < 0$ (predicting the structure to be spontaneously unstable). Adapted, with permission, from [97].

into perovskites to afford novel alloying and **doping** capabilities (Figure 1). Doping of semiconductors like silicon has demonstrated precise control over exotic and attractive material properties, which ultimately has endowed society with most of the essential electronics enjoyed today. This eludes to the unknown auspicious opportunities of perovskite doping that may grant novel device architectures for even greater performance and stability. Herein, we provide an overview of reported advances in the study of the incorporation of metal ions in halide

Glossary

Aliovalent: ion with an oxidation state different than that of the ion it is designed to replace in the crystal lattice. Considering the B site of halide perovskites, ions with an oxidation state of 1+, 3+, or 4+ would all be aliovalent to the 2+ B site.

Dedoping: the introduction of impurities resulting in the shift of the Fermi level towards the center of the bandgap to provide a more intrinsic semiconductor.

Defect passivation: the elimination of defect-induced trap states or reduction of the depth of those trap states to mitigate detrimental nonradiative recombination pathways.

Device hysteresis: when measuring the current–voltage (I–V) characteristic of a solar cell, a voltage is applied, scanning a range across negative and positive bias, and the generated current is measured. If the shape of the measured curve varies when scanning from negative to positive bias and positive to negative bias, the device has a hysteretic effect.

Doping: the controlled addition of impurities to alter the electrical and optical properties of semiconductors. These impurities can change the conductivity of a material and even alter conduction processes between conduction by negative charge carriers (electrons) or positive charge carriers (holes).

Fermi level: the highest energy state occupied by an electron at absolute zero, or the amount of work done to add an electron to the system.

Isovalent: ion with the same oxidation state as the ion it is designed to replace in the crystal lattice. In the case of halide perovskites, for an ion to be isovalent with the A, B, or X site it must have a 1+, 2+, or 1- oxidation state, respectively.

Mid-gap trap density: the density of trap states that lie in the middle of a semiconductor's bandgap. A high trap density deep within the bandgap of a semiconductor can result in adverse nonradiative recombination.

n-Type: a semiconductor material in which the electrical conductivity is dominated by the movement of negatively charged electrons, traditionally resulting from being doped with electron donors. As mentioned in Box 3, the self-doping in halide perovskite can result in the same effect.

perovskites and their role in altering fundamental properties to influence device performance. Throughout the review, the influence of metal ions and their impact on PVSC device performance are summarized in Table 1 (Key Table). Ultimately, we hope to provide a comprehensive review of the effects of metal ions in perovskites to update the field and propel future research in a more informed direction to attain greater fundamental understanding while developing novel perovskite material properties and devices for next-generation technologies.

Influence of Metal Ion Incorporation

On the addition of foreign metal ions to perovskite materials, there are a number of possible outcomes, including alloying, doping, or exclusion during crystallization. Alloyed perovskites are formed by the substitution of a portion of the A, B, or X sites with an appropriate analog to match and maintain the ABX_3 perovskite structure. Most commonly, alloying is achieved via substitution by or the incorporation of an **isovalent** ion. Alloying has afforded the auspicious capability for tuning band structures of perovskites to achieve a range of useful bandgaps, from 1.20 eV to 2.30 eV (Box 1) [4,19–21]. Beyond seeking Pb-free alternatives by entirely replacing the B site with less toxic metals [22] (Figure 1A,B), alloying of isovalent metals like tin (Sn^{2+}) at the B site of ABX_3 materials has proved capable of producing narrow-bandgap materials (attractive for perovskite–perovskite tandem solar devices). However, Sn-based perovskites have been proven to be highly unstable due to their ability to be easily oxidized to Sn^{4+} and introduce significant defects and excess holes [23]. Employing fully inorganic Cs^+-based $CsPbI_{3-x}Br_x$ compositions has afforded PVSCs with improved stability and the potential for application in switchable electronics [24,25]. Alloying organic cations like FA at the A site has also provided exquisite control over the bandgap; however, FA–MA alloyed materials also lack stability due to perovskite systems becoming even more intricate and dynamic when introducing the tumbling and vibrational effects of a FA cation [26,27]. This has led to triple-A-cation (CFM) perovskites comprised of alloying a small amount of Cs^+ with MA and FA for highly stable materials while still achieving favorable band gaps [28,29]. Several studies have established improved stability to be a result of the triple-cation system, enhancing the entropy of mixing, improving the tolerance factor, reducing crystal strain, and restricting the tumbling of FA by increasing the hydrogen-bonding interaction between FA and the I^- of the PbI_6^- octahedron [17,27,28,30,31]. The use of alloying has afforded some of the most efficient PVSCs to date, with the highest certified **power-conversion efficiency (PCE)** reaching 23.7% [10].

The ability of metal ions to alter bandgaps and stability via alloying has allowed excellent progress, but not all metal ions are adequate for alloying. While halide perovskites have been determined to possess unique self-doping capabilities (Box 1), it has been calculated that the incorporation of various **aliovalent** metals into halide perovskites could allow either **p-type** or **n-type** materials through extrinsic doping [32]. It is important to note that, considering the reported studies thus far, the experimental achievement of such doping has proved to return mixed results. In the case of substituting Bi^{3+} for Pb^{2+} at the B site of intrinsically p-type $MAPbBr_3$ single crystals, the additional electrons donated by the 3+ metal upshifts the **Fermi level** and flips the sign of majority charge carriers from p- to n-type while also improving the conductivity [33]. Although the ability to alter carrier concentration is particularly opportune for many electronic devices, the substitution of A, B, or X by an aliovalent ion inevitably introduces undesirable defects into the crystal structure due to the formation of vacancies or altered bonding environments. These defects can introduce electronic **trap states** deep within the bandgap of perovskites capable of hindering the stability and performance PVSCs. Assuming ideal crystallization of Bi-doped $MAPbBr_3$, the substitution by Bi^{3+} at the B site results in one excess e^- and 0.5 Pb vacancies (V_{Pb}) for every Bi atom to give a composition of $CH_3NH_3Pb_{1-x}Bi_{2x/3}V_{Pbx/3}I_3 + e^-_x$ [34]. The detrimental effect of these defects on material properties is evident in Bi^{3+}-doped $MAPbBr_3$, resulting in significant strain-

Power-conversion efficiency (PCE): the percentage of incident power from illumination by light that is effectively converted and extracted as electricity.
p-Type: a semiconductor material which the electrical conductivity is dominated by the movement of positively charged holes. This is traditionally achieved by doping with electron acceptors; however, in halide perovskite it can also be due to the self-doping discussed in Box 3.
Radiative recombination: the annihilation of an electron–hole pair resulting in the emission of a photon.
Trap states: energetic states that lie within the bandgap of semiconductors that can trap either electrons or holes and facilitate detrimental nonradiative recombination processes. These traps are attributed to the presence of defects.

Box 2. Perovskite Bandgap Formation

The electronic structure of the A, B, and X components and their resulting interactions give rise to the properties that have caused perovskite materials to gain so much attention in the past decade. Particularly of interest is the formation and control of bandgaps with low trap density.

The generation of perovskite bandgaps is directly dependent on both the B and the X ion, with mild indirect effects from the A-site cation [5]. For example, in $MAPbI_3$ the formal valence electron structure of Pb^{2+} is $6s^26p^0$ and I^- is $5p^6$. As illustrated in Figure I, the majority of the valence band (VB) is formed by bonding (σ) interactions between I(5p) and Pb(6p) [5,98]. It is critical to note that the VB maximum (VBM) is primarily dictated by the I(5p) orbitals with only minor contributions from the antibonding (σ^*) I(5p)–Pb(6s) due to the stereochemically inactive Pb(6s) cationic lone-pair electrons [5,99,100]. This makes the VBM position highly sensitive to various halides. From Cl to Br to I, with respective orbitals of 3p, 4p, and 5p, the ionization potential decreases to upshift the VBM [5]. By contrast, the conduction band (CB) is generated from the σ^* orbitals of Pb(6p)–I(5p) interactions. In the case of Pb ($6s^26p^0$), the CB minimum (CBM) is formed by the empty 6p orbitals. This unique band structure provides deep-trap tolerance due to σ^* orbitals in the VB that raise the VBM energy and the relativistic effects of the B-site cation lowering the CBM energy to make defect-induced trap states either of shallow energy or resonant within the bands (Figure I).

Studies on the replacement of Pb with Sn or Ge [4,5,19,70,72,101] (all group 14 elements with similar electron structures) and studies of Sb- and Bi-alloyed materials [33,35,50,102] highlight the effects of alloying on the CBM and VBM. Elements with lower atomic weights relative to Pb (Sn, Ge, and Sb) provide greater ns^2 contribution to the σ^* characteristic of the VBM, raising its energy. By contrast, Bi has a higher atomic weight than Pb and results in increased spin-orbital coupling to favorably lower the CBM. Thus, achieving a balance of low trap density and stability has proved to be quite troublesome. This effect is evident from the instability of Sn and Ge in a 2+ oxidation state and the high defect density resulting from the incorporation of Bi^{3+}.

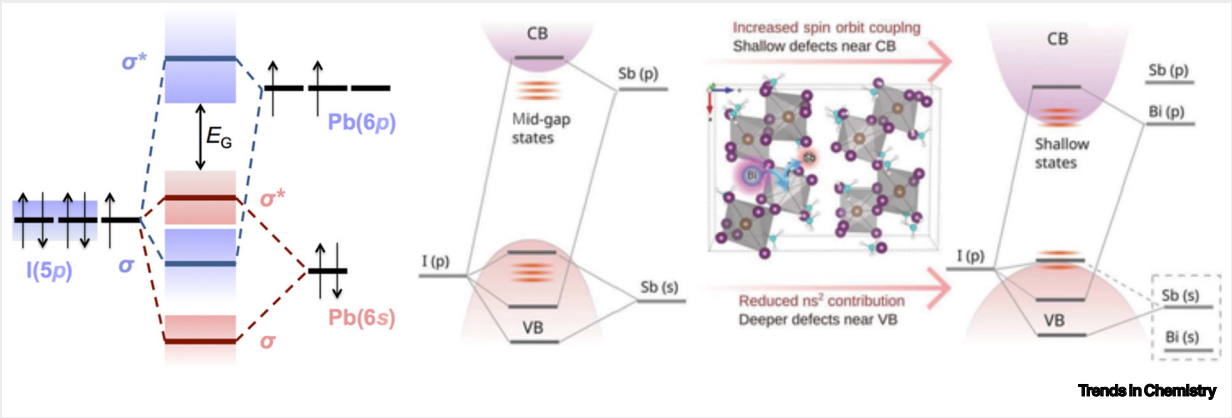

Figure I. The Formation of Valence and Conduction Bands in $MAPbI_3$ from Bonding (σ) and Antibonding (σ*) Orbitals Shown Relative to the Isolated s and p Atomic Orbital Energies of Halide and Metal. The resulting effect of electronic structure on mid-bandgap defects. Adapted, with permission, from [98,102].

induced instability and recombination centers capable of facilitating adverse recombination pathways [33,35–37].

Although undesirable for PVSC application, the incorporation of metal ions resulting in recombination centers has been effectively utilized to tune the emissive properties [e.g., PL quantum yield (PLQY)] of perovskite nanocrystals (NCs) for LEDs [8,38]. A wide array of lanthanide and transition metals have been reported to incorporate into inorganic-based perovskite NCs [30,39–43]. In these perovskite-host structures, excitons generated in inorganic frameworks exhibit fast and efficient exciton energy transfer to the incorporated metal ion to facilitate **radiative recombination** (Figure 1C) [38]. Tuning the metal ion has then been able to control the wavelength of emitted light to produce a remarkable color gamut while also improving the PLQY (Figure 1D), making metal ion incorporation an attractive avenue for the development of next-generation LEDs.

Although some metals have shown essentially no capability to incorporate into perovskite structures, their effect on perovskite properties is far from inert. From even some of the earliest

Box 3. Self-Doping in Perovskites

Self-doping in hybrid perovskites was first observed and described for $MAPbI_3$ films by Q. Wang and colleagues [103]. It was determined that $MAPbI_3$ films prepared from a precursor with perfect stoichiometry of 1 MAI to 1 PbI_2 showed heavily n-doped properties with an electron carrier concentration of 2.8×10^{17} cm^{-3}. However, a lightly p-doped film with a hole carrier concentration of 4.0×10^{16} cm^{-3} was formed when a stoichiometry of 1 MAI to 0.3 PbI_2 was used. The ability to shift between n- and p-type materials purely by adjusting the precursor ratio demonstrated the composition dependence of the self-doping effect in OIHPs where Pb^{2+}-rich films result in n-doped materials and p-doped materials result from MA-rich films. It is suspected that a precursor with excess MAI induces a significant number of Pb (V_{Pb}) and I (V_I) vacancies, but the p-type nature is expected to be primarily due to V_{Pb} due to a much lower formation energy from previous calculations [104]. The n-type nature of films with a 1-to-1 stoichiometry is then attributable to the formation of V_I and MA vacancies (V_{MA}) due to evaporation during the thermal annealing process that is standard for OIHP thin films. Calculations show that V_I has a lower activation energy relative to V_{MA}, suggesting that V_I also contributes significantly to the n-type nature of films with 1-to-1 stoichiometry [103,104]. Ultimately, these experimental results match well with the computational work of W. Yin and colleagues suggesting n-doping in PbI_2-rich films and p-doping in those with PbI_2 deficiency [104]. Interestingly, it was found that additional annealing of the p-doped films was able to revert them to n-doped, while surface treatment with a solution of MAI was able to convert the n-doped films to p-type (Figure I) [103]. This demonstrates a materials processing dependence of self-doping in OIHPs and may be a source of some discrepancies between reports of attempts to incorporate the same metal into the same composition.

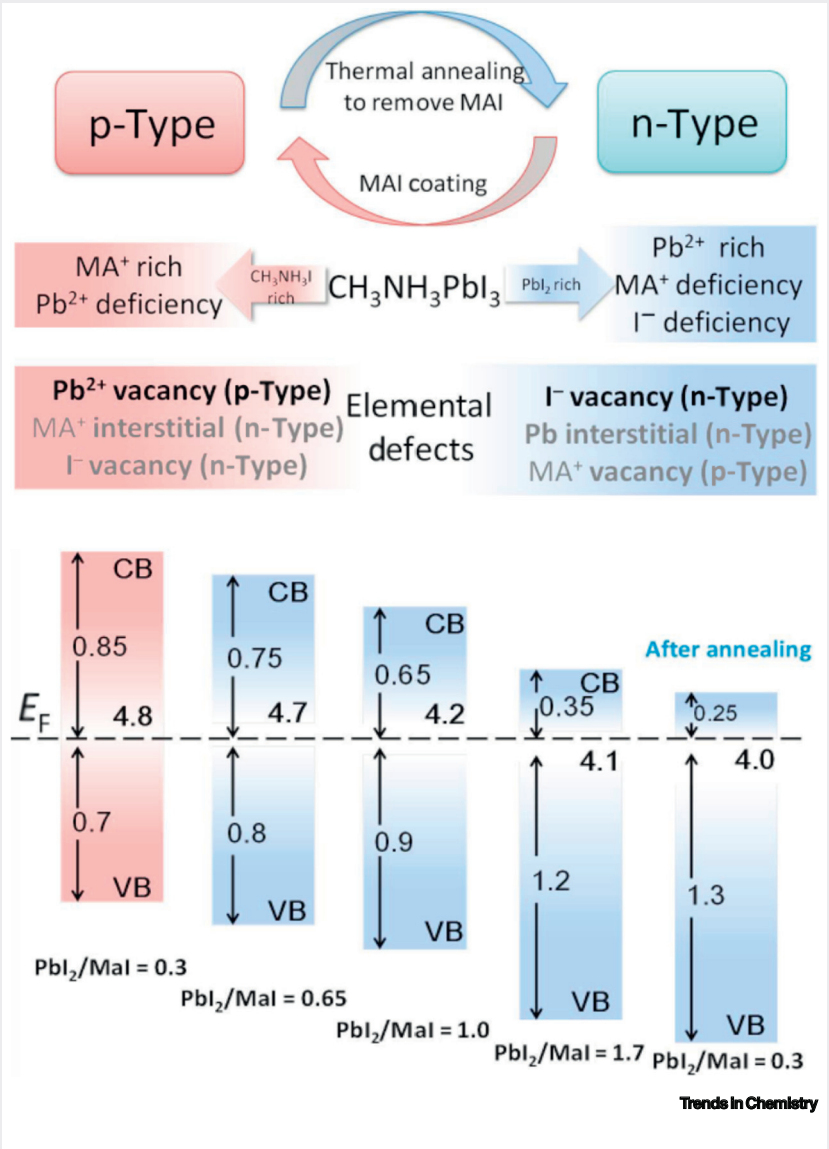

Figure I. Schematic for Resulting Conductivity Based on Composition, Point Defects, and Elemental Defects (Those Listed in Gray Are Less Likely to Be Formed in Films) and the Resulting Shift in Fermi Level Due to Composition and Annealing. Adapted, with permission, from [103].

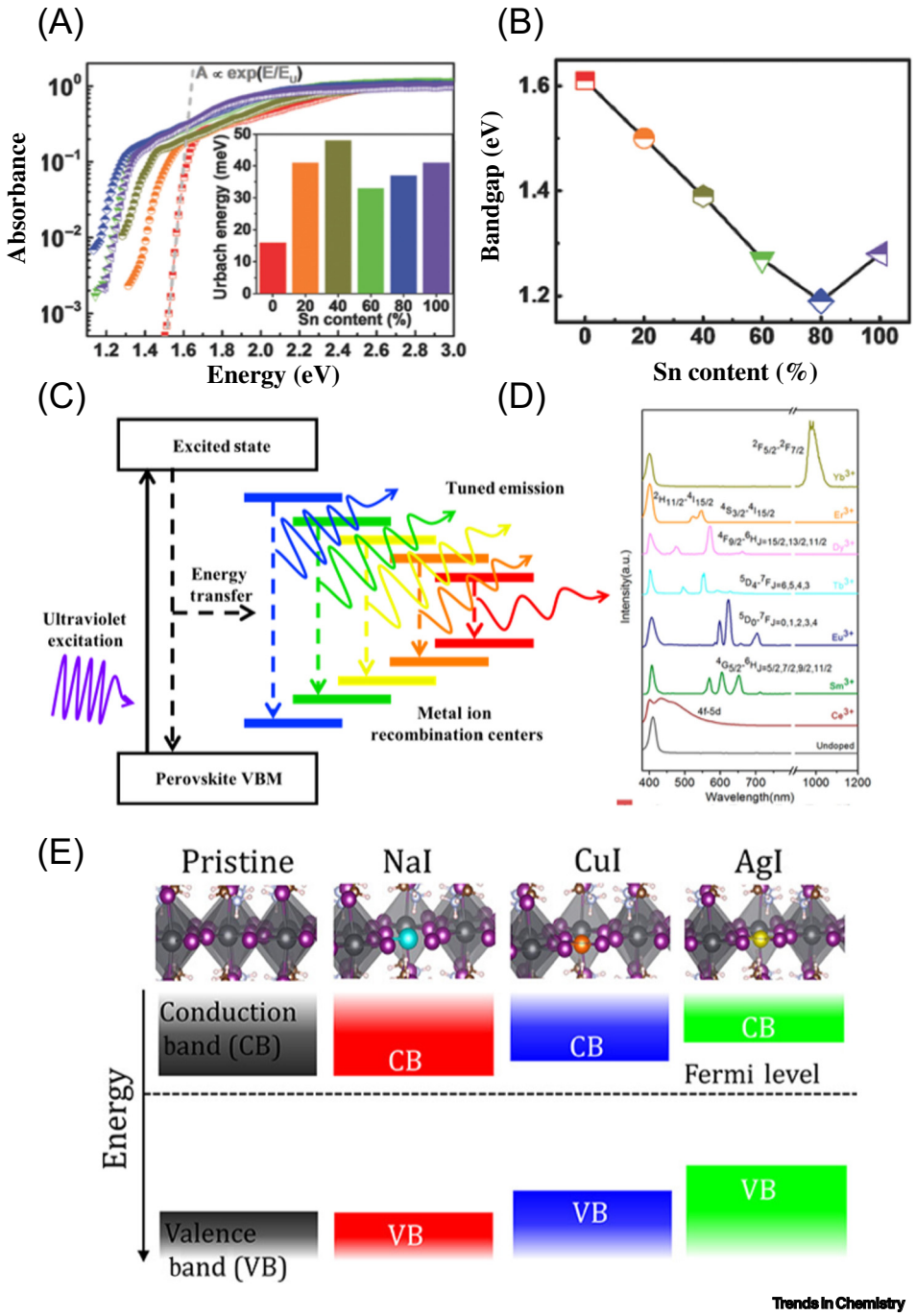

Figure 1. The Alloying and Doping of Halide Perovskites via Incorporation of Metal Ions. (A) The absorption spectra and calculated Urbach energies for a range of Sn^{2+}-alloyed halide perovskites. (B) The resulting bandgap modulation using Sn^{2+} alloying. (C) Schematic of the fast transfer of exciton energy to metal ion-induced recombination centers to provide tunable emission in a wide color gamut. (d) The emission spectra of $CsPbCl_3$ nanocrystals (NCs) doped with various lanthanide ions demonstrating tunable emission. (E) The Fermi level shift in $MAPbI_3$ with the incorporation of Cu^+ and Ag^+. Adapted, with permission, from [4,39,59].

Key Table

Table 1. Influence of Metal Ion Incorporation on the Performance of PVSC Devices and Proposed Origin of Effects[a]

Metal added	Composition	mol% Metal	Device/sample	PCE	Cause	Refs
Al^{3+} [Al(acac)$_3$]	$MAPbI_3$	0.15	PVSC (p-i-n)	17.1 → 19.1	Improved V_{oc} and J_{sc} due to higher-quality films with reduced microstrain	[49]
Sb^{3+} (SbI_3)	$MAPbI_3$	1	PVSC (n-i-p)	13.1 → 15.5	n-Doping resulting in greater built-in potential, improved electron transport with long diffusion lengths	[50]
Bi^{2+} (BiI_2)	FAPbI3	5	PVSC (n-i-p)	13.02 → 17.78	Lower resistance as well, improved stability of alpha-phase	[51]
In^{3+} ($InCl_3$)	$MAPbI_3$	3	PVSC (p-i-n)	12.29 → 17.34	Induces multiple preferential growth orientations beneficial to charge transport	[53]
Eu^{3+} [Eu(acac)$_3$]	$(Cs_{0.14}FA_{0.43}MA_{0.43})Pb(I_{2.6}\ Br_{1.4})(Cl)$	0.15	PVSC (n-i-p)	18.5 → 20.7	Lower defect density and improved stability due to redox shuttle of Eu^{3+}/Eu^{2+}	[56]
Ag^{+} (AgI)	$MAPbI_3$	3–8	PVSC (n-i-p)	16.7 → 20.0	Dedoping from n-type to intrinsic, reduced disorder, reduced nonradiative recombination rate, passivation	[59]
Cu^{+}(CuI)	$MAPbI_3$	3–8	PVSC (n-i-p)	16.7 → 19.2	Dedoping from n-type to intrinsic, reduced disorder, reduced nonradiative recombination rate, passivation	[59]
Na^{+} (NaI)	$MAPbI_3$	3.0	PVSC (n-i-p)	16.7 → 20.5	Reduced disorder, reduced nonradiative recombination rate, passivation	[59]
		1.0	PVSC (n-i-p)	15.56 → 18.16	Larger grain sizes reducing grain boundaries and trap states, enhancing built-in potential	[62]
		0.25	PVSC (p-i-n)	12.8 → 14.54	Improved grain sized and crystallinity	[91]
K^{+} (KI)	$MAPbI_3$	N/R	PVSC (n-i-p)	15.56 → 17.81	Larger grain sizes reducing grain boundaries and trap states, enhancing built-in potential	[62]
		0.5	PVSC (p-i-n)	12.8 → 15.31	Improved grain sized and crystallinity.	[91]
Hg^{2+} (HgI_2)	$MAPbI_3$	10	PVSC (p-i-n)	8.6 → 11.9	Increased grain size	[67]
Co^{2+} [Co(OAc)$_2$]	$MAPbI_3$	1.6	PVSC (p-i-n)	16.6 → 17.2	Improved V_{OC} due to shift in Fermi level	[75]
Fe^{2+} (FeI_2)	$MAPbI_3$	10.0	PVSC (p-i-n)	10.3 → 0.9	Half-metallic behavior shorting the device	[77]
Cd^{2+} (CdI_2)	$Cs_{0.05}MA_{0.15}FA_{0.8}PbI_{2.55}Br_{0.45}$	N/R	PVSC (n-i-p)	~21.5 →~21.5	Dramatically increased stability due to suppression of defects	[78]
Ca^{2+} (CaI_2)	$MAPbI_3$	0.5	PVSC (p-i-n)	16.1 → 19.3	Improved crystallinity and effective defect passivation	[83]
Ba^{2+} (BaI_2)	$MAPbI_3$	3	PVSC (n-i-p)	11.8 → 14.0	Improved crystallinity and grain morphology	[85]
Sr^{2+} (SrI_2)	$MAPbCl_3$	1.0, 10.0	PVSC (n-i-p)	13.7 → 10.3 → 0.05	Poor morphology and likely large defect density	[85]
Sr^{2+} ($SrCl_2$)	$MAPbI_3$	10	PVSC (n-i-p)	13.0 → 15.9	Control of crystallization for lower defect density	[92]
Mn^{2+} ($MnCl_2$)	$CsPbI_2Br$	2	PVSC (p-i-n)	11.88→13.47	Large-aspect-ratio grain sizes, passivation of grain boundaries	[90]
Rb^{+} (RbI)	$MA_{17}FA_{83}PbI_3$	1	PVSC (n-i-p)	17.5 → 20.3	Passivation of grain boundaries by Rb-rich phase	[93]

[a]Note that the table is not exhaustive but contains recent reports with the most significant change attributable to similar effects in earlier reports of the same metal.

studies of crystallization, it has been evident that the presence of metal ions can influence the crystallization of materials [44]. It is now understood that impurity ions can either impede or facilitate the growth of crystals in the direction of selective planes by adsorbing to a growing surface and inducing steric hindrance or lowering the surface energy to catalyze growth [45–48]. J. Wang and colleagues have reported preferential growth of the (110) direction on the addition of small amounts of aluminum (Al^{3+}) (Figure 2A). While Al^{3+} is nearly entirely expelled to surfaces and grain boundaries during crystallization, the resulting perovskite films exhibit improved crystallinity by a ~0.5% contraction in lattice spacing and reduced electronic disorder and strain in the bulk (Figure 2B) [49]. Improved crystallinity is thought to be indicative of Al^{3+} inducing more ordered coordination of halides to Pb^{2+} to effectively reduced iodide vacancies (V_I) in the bulk [49], which we suspect may also influence the self-doping process. The ability to suppress defects in the bulk through controlled crystallization while Al^{3+} localized at grain boundaries can provide additional passivation of surface defects (similar to the effects reported for other additives and metals) demonstrates the potential benefit of multifunctional metal ions.

Influence of Aliovalent High-Valency Metals

The ability to alter the Fermi level of semiconductors using higher-valency aliovalent ions, like Bi^{3+} discussed above, is particularly enticing for the potential doping of ABX_3 perovskite materials. In addition to Bi^{3+}, Zhang and coworkers confirmed the incorporation of antimony (Sb^{3+}) to provide direct n-doping in $MAPbI_3$ [50]. The substitution of Pb^{2+} by aliovalent Sb^{3+} was confirmed to generate vacancies that could act as deep charge traps. The generation of defects by aliovalent metals introduces significant local strain that hinders the stability of perovskite materials [35,37]. To maximize the charge-carrier density without reaching a detrimental trap density, the concentration of incorporated antimony (Sb^{3+}) was tuned to provide a 30% increase in carrier density (Figure 2D). Improved carrier density and upward shift of the Fermi level resulted in a 0.095-V increase of open-circuit voltage (V_{oc}) and a PCE of 15.6%, compared with the 13.1% of their pristine $MAPbI_3$ devices [50]. Interestingly, contrary to the high defect density generated by the incorporation of Bi^{3+} in $MAPbBr_3$, it is reported to improve the stability of $CsPbI_3$ and $FAPbI_3$ materials, demonstrating that the influence of Bi^{3+} is dependent on composition [51,52]. Gold (Au^{3+}) and indium (In^{3+}) have also been reported to be capable of incorporation [33], but their doping effects have yet to be fully characterized and warrant additional research.

Besides doping effects, metals like Al^{3+} can provide tremendous morphological control to improve further the PCE of PVSCs from 17.1% to 19.1% [49]. The incorporation of indium (In^{3+}) has also been reported by Wang and colleagues to influence morphology by facilitating preferential growth of grains in several orientations [53]. While exhibiting small grains with a variety of preferred growth orientations, incorporation of In^{3+} was still reported to reduce defect density by improving the ordering of MA within the perovskite structure and PVSCs, with improved PCE [49,53].

The incorporation of aliovalent rare earth (RE) metals (i.e., Ce^{3+}, Sm^{3+}, Eu^{3+}, Tb^{3+}, Dy^{3+}, Er^{3+}, and Yb^{3+}) has afforded control over the emissive properties of $CsPbBr_{3-x}Cl_x$ NCs [30,39–43]. As determined from X-ray diffraction experiments, NCs with RE metals exhibit smaller lattice spacing while maintaining the same tetragonal phase of pristine NCs, representative of successful substitution of Pb^{2+} with smaller RE metal cations [39]. However, few RE metals have been reported in perovskite thin films or single crystals, making it an attractive direction as europium (Eu^{3+}) is reported to stabilize $CsPbI_3$ thin films as well as producing highly efficient $CsPbIBr_2$ solar cells [54,55]. Most recently, L. Wang and colleagues reported the capability of Eu^{3+} to be used as a tool to impart high operational stability [56]. It was determined that Eu^{3+} is able to act as a

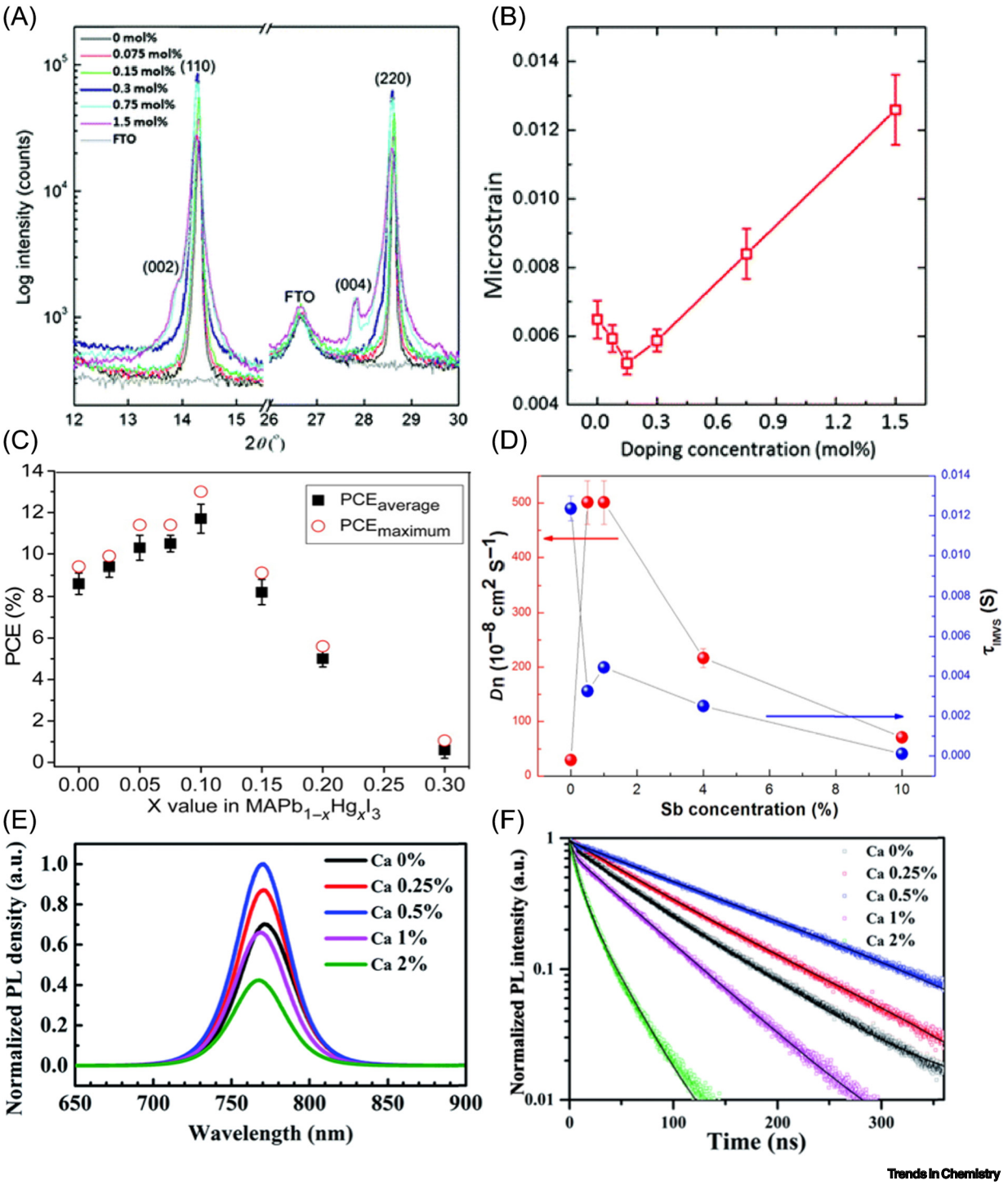

Figure 2. Tuning Metal Ion Concentration to Improve a Variety of Material Properties and Device Characteristics. (A) X-ray diffraction patterns showing preferential growth orientations with improved crystallinity on Al^{3+} incorporation. (B) The microstrain resulting from the addition of Al^{3+} calculated from (A), with a minimum occurring at 0.15 mol%. (C) Power-conversion efficiency (PCE) of perovskite solar cells (PVSCs) showing Hg^{2+}. (D) Influence of n-type doping by Sb^{3+} on the diffusion coefficient (D_n) and electron lifetime (η), suggesting an optimum concentration of 1 mol% Sb^{3+}. (E) The ability of calcium to improve steady-state photoluminescence (PL) intensity, which is maximized with 0.5 mol% Ca^{2+}. (F) Maximizing the PL lifetime with the incorporation of 0.5 mol% Ca^{2+}. Adapted, with permission, from [49,50,67,83].

redox shuttle between Eu^{3+} and Eu^{2+} to limit the Pb^0 and I^0 resulting from degradation. This uncovers another highly attractive application for metal ions in perovskite materials that should be further explored.

Influence of Aliovalent Low-Valency Metals

Outside Cs^+ and rubidium (Rb^+), discussed below, the ability to incorporate other alkali metals [sodium (Na^+) and potassium (K^+)] into the perovskite lattice and their resulting effect have provided mixed results over time. In the first work reporting the effect of Na^+, C. Bi and colleagues found that Na^+ originating from the substrate was capable of diffusing into grain boundaries of perovskite films [57]. Thermal admittance spectroscopy was used to determine that these Na^+-enriched grain boundaries significantly lower the defect density of the film, suggesting efficient passivation of defect-induced trap states. Most notably, passivation of mixed halide compositions by K^+ has afforded near-unity internal PLQY by stabilizing bromide (Br^-) ions to mitigate phase segregation and instability [58]. Although Na^+ and K^+ are seemingly capable of penetrating into the perovskite bulk [59,60], they are still thought to be concentrated at the surface and grain boundaries of perovskite to provide efficient defect passivation [58]. In addition to passivation, the incorporation of alkali metals is also able to stabilize $CsPbBr_3$ compositions [61]. The doping capability of Na^+ in $MAPbI_3$ was first calculated by Shi and colleagues [32] and later experimentally demonstrated by Y. Yang and coworkers, reporting Na^+ capable of switchable doping of $MAPbI_3$ films from n-type to p-type [60]. The concentration of holes was determined to increase with Na^+ concentration, but mobility dropped due to Na^+ acting as scattering centers. In addition to this doping effect, there is a blue shift in the PL of samples containing Na^+, which was assumed to be indicative of bandgap widening due to the small Na^+ cation distorting and shrinking the $MAPbI_3$ crystal lattice [60]. However, we believe that because the shift is ≤10 nm, it is likely to be due to the reported passivation effect of Na^+ and not lattice constriction. However, M. Abdi-Jalebi and coworkers later showed an expansion of the lattice with incorporation of Na^+ but determined no doping effect on the Fermi level due to the complete overlap of orbitals with band structures [59]. Here Na^+ is also measured to be incorporated into the bulk, although it was found to primarily reside at grain boundaries, demonstrating inability to significantly penetrate the crystal lattice [59], consistent with earlier works [62,63]. Although numerous studies have used XPS to show that Na^+ and K^+ seem to exist to some extent in the bulk, XPS probes only the top 10 nm of the samples, making their definite location up for debate.

One possibility proposed by D. Son and colleagues is that these alkali metals are incorporated into the interstitial sites of perovskite and reported that **device hysteresis** decreased to negligible levels from Li → Na → K before reappearing and increasing from K → Cs → Rb [64]. It was calculated that K^+ is the most energetically favored to occupy interstitial sites and suppress the migration of Frenkel defects. This was reported to effectively eliminate hysteresis in PVSCs, reduce the defect density of both the surface and the bulk, and improve stability [64]. The size of K^+ is thought to make it compatible with any composition of perovskite, while imparting no doping effects. The passivation of mixed halide compositions by K^+ has been particularly effective by stabilizing bromide (Br^-) ions, which can easily migrate to result in phase segregation and instability [58]. To further complicate our state of understanding, D. Kubicki and colleagues used solid-state ^{13}C, ^{14}N, and ^{39}K NMR to show K^+ is not incorporated into the lattice [65]. The ^{39}K spectrum shows potassium to exist only in the form of unreacted KI and no substantial shift of peaks in either the ^{13}C or the ^{14}N spectrum suggests no interaction between the organic cations and K^+ [65].

Beyond alkali metals, M. Abdi-Jalebi and colleagues later reported the partial aliovalent incorporation of the monovalent transition metals copper (Cu^+) and silver (Ag^+) [59]. As shown in

Figure 1E, both Cu^+ and Ag^+ experimentally exhibit the ability to reduce the n-type character of control perovskite films via downshifting the Fermi level. Such a shift in the Fermi level is likely to be due to the compensation for halide vacancies by substitutional doping of the B site by aliovalent metals. This is further validated by an order-of-magnitude drop in conductivity compared with control films. Measurement of samples containing Cu^+ and Ag^+ showed that this so-called **dedoping** effect also manifested in cleaner bandgaps and lower energetic disorder. It was again observed that the incorporation of these metals was capable of influencing the crystallization process, producing a preferred growth orientation and a surface rich with I^- that may also influence doping. Although the ionic radii of both Cu^+ (91 pm) and Ag^+ (129 pm) are smaller than that of Pb^{2+} (133 pm), their incorporation expanded the unit cell of both doped PbI_2 and $MAPbI_3$, contrary to the expected lattice contraction when substituting in smaller ions [59,66]. It was proposed the expansion may release strain attributed to the lattice rearrangement or defects caused by the combination of substitutional and interstitial doping by aliovalent metals [59]. Although additional strain is induced, Cu^+ and Ag^+ have been demonstrated to have little impact on device performance [67].

Influence of Isovalent Metals

To date, the substitution of the A- and B-site cations via alloying with their respective isovalent metals has been a central focus in the field of compositional engineering, with the thrust to further improve stability and electronic properties as well as develop Pb-free materials. Like Cs, which has proved effective in providing highly stable materials through A-site alloying [24], alloying by the slightly larger Rb^+ has recently been demonstrated by M. Zhang and coworkers to stabilize FA- and FA/MA-based compositions. Rb^+ was initially reported to incorporate into other single-, double, and triple-cation compositions, but rapid phase segregation results in $RbPbI_3$, $RbI_{1-x}Br_x$, and $Cs_{0.5}Rb_{0.5}PbI_3$ at the surface and grain boundaries of films [68]. These inorganic Rb-rich layers have been proposed to passivate the perovskite surface and grain boundaries and improve moisture stability [65]. The use of other wide-bandgap materials to passivate the surface and grain boundaries of perovskite has been proved to improve stability and effectively suppress trap-induced charge recombination to afford improved device performance [18]. It is also evident that this may affect the resulting carrier concentration of films [69]; whether that is through passivation of surface defects, controlling composition, or true direct doping should be further elucidated.

As for exploring the influence of metals isovalent to the 2+ B site, in addition to the work on Sn-alloyed narrow-bandgap materials, germanium (Ge^{2+}) was also initially suggested as an attractive candidate for developing Pb-free organic–inorganic hybrid perovskites [70,71]. However, these perovskites exhibit extremely poor efficiencies of <1% in pure Ge-based PVSCs and state-of-the-art Pb-free Ge–Sn-alloyed devices attain only 4.48% (6.90% after storage for 72 h) [72,73]. Interestingly, an entirely inorganic Ge-alloyed perovskite ($CsPb_{1-x}Ge_xI_2Br$) material processed in ambient atmosphere was recently reported with lower trap density and improved recombination lifetimes, despite a reduction in the average grain size [74]. These Ge-alloyed perovskites produced devices with high V_{oc} of up to 1.34 eV and PCE of 10.8%, stable in atmosphere with high humidity and no encapsulation for 7 h. Although Sn and Ge were predicted to be easily incorporated via substitution of Pb^{2+}, their resulting instability and relatively low performance led to work on a wide variety of other isovalent metals.

M. Klug and colleagues were the first to provide a systematic experimental characterization of the partial substitution of Pb^{2+} at the B site by Mg^{2+}, Mn^{2+}, Fe^{2+}, Co^{2+}, Ni^{2+}, Cu^{2+}, Zn^{2+}, Sr^{2+}, and Sn^{2+} [75]. For devices with metal added in low concentrations (1.5 % substitution of Pb^{2+}), all but Fe^{2+} maintained or improved device performance. However, with the exception of Sn^{2+}

and Cu^{2+}, substituting ~6% of Pb^{2+} proved to be the threshold before significant lowering of J_{sc} [75]. We believe this tolerance level can account for the detrimental effects reported when adding metals at concentrations up to 10 mol% [67]. It should be noted that Fe^{2+} proved to be detrimental to device performance at even the most minute concentrations [76], consistent with the work done at roughly the same time using DFT to attribute diminished device performance to a half-metallic behavior induced by Fe^{2+} [77]. $MAPbI_3$ films and devices with incorporated Co^{2+} were studied in more thorough detail, showing the ability to tune the Fermi level and valence band edge without altering the bandgap to improve the band alignment between $MAPbI_3$ and the hole-transport layer (PEDOT:PSS) [75]. The incorporation of the smaller Co^{2+} cation also induced a change in crystal structure from cubic to tetragonal at room temperature, demonstrating lattice contraction. Further increasing the Co^{2+} content continues to reduce lattice spacing [75], indicative of Co^{2+} incorporation effectively reducing strain [36].

Cd^{2+} has also shown successful incorporation into the perovskite lattice via substitution of Pb^{2+} [78–80]. Given the reduction in lattice strain by substitution of Pb^{2+} by smaller Cd^{2+}, it is calculated to also raise the formation energy for I^- vacancies to effectively suppress defect formation and improve stability [78]. The suppression of defects may be further supported by Z. Almutawah and colleagues reporting the use of Cd^{2+} and Zn^{2+}, both with similar electron configurations, to influence the grain growth and crystallinity with small amounts added to the precursor solution [76]. Incorporation of Zn^{2+} showed promising stability but the PCE of fresh devices was slightly decreased [76,78]. The addition of mercury (Hg^{2+}) has exhibited comparable or improved time-zero PCE but unexpectedly degraded over only a few days (Figure 2C) [67,78]. Rapid Hg-induced degradation can be attributed to the reduction of Hg^{2+} to Hg^+, which is likely to generate additional I^- vacancies [81]. Although Zn^{2+}, Cd^{2+}, and Hg^{2+} have similar electron configurations, we believe that their strength of bonding with I^- and thus greater suppression of defects and structural stability should follow the same trend as their polarization power, Cd > Zn > Hg, which is consistent with reported data. The ability to control crystallinity and improve performance and stability has also been reported for low concentrations of barium (Ba^{2+}) (<3.0 mol%) and calcium (Ca^{2+}) (≤0.5 mol%) [82,83]. Although the position of Ca^{2+} is unclear, it is presumed to be primarily located at grain boundaries due to the exceptional passivation of defects [83], similar to K^+. The influence of Ca^{2+} on crystallization coupled with its effective passivation and improved built-in potential has resulted in devices with improved performance and long-term stability (Figure 3).

Although all isovalent metals reviewed to this point have been suspected of incorporating into perovskites, being classified as isovalent does not immediately qualify a specific metal to be incorporated (Box 1). Pérez-del-Rey and coworkers reported that the addition of strontium (Sr^{2+}) to $MAPbI_3$ results in films with small grains that XPS suggests to be wrapped in wide bandgap SrO (5.7 eV), $SrCO_3$ (4.3 eV), and $Sr(C_2H_3O_2)_2$ with probably no Sr^{2+} incorporated into the bulk [84]. The resulting Sr-based interlayers prove capable of defect passivation and altering the surface dipole to improve electron extraction, resulting in devices with extremely high FF 84.7% compared with the 77% of pristine $MAPbI_3$. Due to the insulating nature of the interlayers, there is a drastic drop in performance as the feed concentration of Sr^{2+} and resulting interlayer thickness increase [84,85]. E. Yao and colleagues also elucidated an increase in recombination rates with the incorporation of Sr^{2+}, possibly indicative of defects or recombination centers generated by Sr^{2+} [86].

Similar to the rare earth metals discussed above, Mn^{2+}, Zn^{2+}, and Cd^{2+} have also proved to be highly effective in improving the optical properties of $CsPbX_3$ NCs, allowing tunable emission in a wide color gamut, showing great potential in LEDs [38,87–89]. Additionally, Bai and colleagues reported Mn^{2+} to incorporate at the interstitial sites of $CsPbI_2Br$ thin films to provide grains with

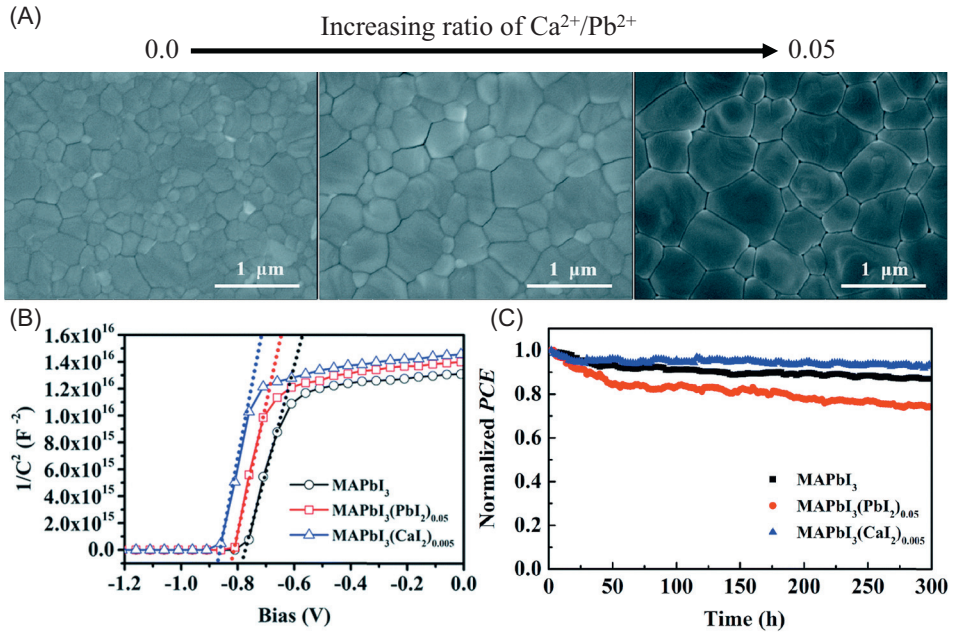

Figure 3. Influence of Calcium on Grain Size and Perovskite Solar Cell (PVSC) Performance. (A) Scanning electron microscopy images showing the influence of increasing Ca^{2+} content on the grain size of thin film. (B) Mott–Schottky plots presenting the greater built-in potential of $MAPbI_3(CaI_2)_{0.005}$ films compared with pristine $MAPbI_3$ and $MAPbI_3(PbI_2)_{0.05}$. (C) Long-term stability of inverted PVSCs based on the pristine $MAPbI_3$, $MAPbI_3(PbI_2)_{0.05}$, and $MAPbI_3(CaI_2)_{0.005}$ films, respectively, measured in an N_2-filled glovebox under continuous light soaking and maximum power point tracking. Adapted, with permission, from [83].

extremely large aspect ratios of up to 8 on the addition of 2 mol% Mn^{2+}, resulting in good stability and a record efficiency for $CsPbI_2Br$ solar cells of 13.47% [90].

Z. Yong and colleagues were able to demonstrate not only the incorporation of nickel (Ni^{2+}) into $CsPbCl_3$ NCs but also vastly improved short-range ordering in the NCs [8]. Measuring the extended X-ray absorption fine structure (EXAFS) showed that Ni^{2+} has octahedral coordination indicative of incorporation into the lattice while also inducing improved coordination around both Pb^{2+} and Cs^+. Through density functional theory (DFT) calculations, the improved coordination has been attributed to a Ni^{2+} imparting a large increase in defect formation energies, particularly Cl^- vacancies known to be a source of deep traps, culminating in a remarkable improvement in the PLQY of $CsPbCl_3$ NCs from 2.4% to 96.5% [8].

Concluding Remarks

The incorporation of metal ions has undoubtedly exhibited the ability to drastically influence the optoelectronic and physical properties of perovskite materials. Some metal ions have already proved to be highly effective in alloying as well as passivation to afford PVSCs with record efficiencies and stability. Additionally, the initial doping effects of metal ion incorporation reveal a world of potential for novel control of electronic properties allowing state-of-the-art device architectures and even additional applications that may have yet to be realized. Although our understanding of whether metals are successfully incorporated into the perovskite structure as well as their mechanism for governing properties remains in its infancy, these reviewed works foretell the use of added metal ions being critical in further improvement and commercialization of perovskite-based devices.

Outstanding Questions

If incorporated into the bulk of halide perovskite materials, what is the true position of metal ions?

Can controlled preferential growth of halide perovskites be designed by careful selection of metal ions?

How does altering perovskite composition influence the alloying, doping, or passivation capabilities of a given metal ion?

Is the doping of halide perovskites by metal ions primarily attributable to the direct contribution of charge carriers by the metal or a compositional self-doping effect from altered crystallization?

What types of strain are metal ions capable of either inducing or relieving in halide perovskite materials?

Moving forward, to fully exploit the potential that metal ion incorporation presents, research must be done to clarify and improve fundamental understanding on the role of metal ions in crystallization, their doping capability, the true position of metal ions, and how these differ with altered perovskite compositions (see Outstanding Questions). Although computational methods are improving and would be attractive for predicting such effects, they cannot always be reliable due to the well-accepted dependence of perovskite properties on material processing and the general complexity of such systems. Thus, to develop our understanding, we believe that future research must be heavily experimental and rely on calculations to assist in understanding outcomes. Furthermore, as all ions reported so far have demonstrated some capacity to change material properties, performance, and particularly the crystallization process, it seems that there is no reason to limit research efforts to only particular groups of the periodic table. Future studies on different metals and various compositions will be critical to clearly elucidate the mechanism for altering perovskite properties and ultimately facilitate improvements in the performance and stability of PVSCs, LEDs, and X-ray or gamma-ray detectors.

Acknowledgments

J.H. and P.R. acknowledge and thank the support of the National Science Foundation (NSF) (grant no. DMR-1801741).

References

1. Dong, Q. *et al.* (2015) Electron-hole diffusion lengths > 175 μm in solution-grown $CH_3NH_3PbI_3$ single crystals. *Science* 347, 967–969
2. Shi, D. *et al.* (2015) Low trap-state density and long carrier diffusion in organolead trihalide perovskite single crystals. *Science* 347, 519–522
3. Hu, M. *et al.* (2015) Stabilized Wide Bandgap $MAPbBr_xI_{3-x}$ perovskite by enhanced grain size and improved crystallinity. *Adv. Sci. (Weinh.)* 3, 1500301
4. Zhao, B. *et al.* (2017) High open-circuit voltages in tin-rich low-bandgap perovskite-based planar heterojunction photovoltaics. *Adv. Mater.* 29, 1604744
5. Walsh, A. (2015) Principles of chemical bonding and band gap engineering in hybrid organic–inorganic halide perovskites. *J. Phys. Chem. C* 119, 5755–5760
6. Richter , J.M. *et al.* (2016) Enhancing photoluminescence yields in lead halide perovskites by photon recycling and light out-coupling. 7, 13941
7. Shin, S.S. *et al.* (2015) High-performance flexible perovskite solar cells exploiting Zn_2SnO_4 prepared in solution below 100°C. *Nat. Commun.* 6, 7410
8. Yong, Z.J. *et al.* (2018) Doping-enhanced short-range order of perovskite nanocrystals for near-unity violet luminescence quantum yield. *J. Am. Chem. Soc.* 140, 9942–9951
9. Deng, Y. *et al.* (2018) Surfactant-controlled ink drying enables high-speed deposition of perovskite films for efficient photovoltaic modules. *Nat. Energy* 3, 560–566
10. NREL (2019) *Best Research-Cell Efficiencies*. National Renewable Energy Laboratory
11. Dou, L. *et al.* (2014) Solution-processed hybrid perovskite photodetectors with high detectivity. *Nat. Commun.* 5, 5404
12. Wei, H. *et al.* (2016) Sensitive X-ray detectors made of methylammonium lead tribromide perovskite single crystals. *Nat. Photonics* 10, 333–339
13. Bao, C. *et al.* (2017) Low-noise and large-linear-dynamic-range photodetectors based on hybrid-perovskite thin-single-crystals. *Adv. Mater.* 29, 201703209
14. Lin, K. *et al.* (2018) Perovskite light-emitting diodes with external quantum efficiency exceeding 20 per cent. *Nature* 562, 245–248
15. Cao, Y. *et al.* (2018) Perovskite light-emitting diodes based on spontaneously formed submicrometre-scale structures. *Nature* 562, 249–253
16. Jiang, Q. *et al.* (2019) Surface passivation of perovskite film for efficient solar cells. *Nat. Photonics* Published online April 1, 2019. https://doi.org/10.1038/s41566-019-0398-2
17. Li, Z. *et al.* (2016) Stabilizing perovskite structures by tuning tolerance factor: formation of formamidinium and cesium lead iodide solid-state alloys. *Chem. Mater.* 28, 284–292
18. Ran, C. *et al.* (2018) Defects in metal triiodide perovskite materials towards high-performance solar cells: origin, impact, characterization, and engineering. *Chem. Soc. Rev.* 47, 4581–4610
19. Noel, N.K. *et al.* (2014) Lead-free organic–inorganic tin halide perovskites for photovoltaic applications. *Energy Environ. Sci.* 7, 3061–3068
20. Noh, J.H. *et al.* (2013) Chemical management for colorful, efficient, and stable inorganic–organic hybrid nanostructured solar cells. *Nano Lett.* 13, 1764–1769
21. Eperon, G.E. *et al.* (2014) Formamidinium lead trihalide: a broadly tunable perovskite for efficient planar heterojunction solar cells. *Energy Environ. Sci.* 7, 982–988
22. Wang, R. *et al.* (2019) Opportunities and challenges of lead-free perovskite optoelectronic devices. *Trends Chem.* xx, 1–12 Published online 17 May 2019. https://doi.org/10.1016/j.trechm.2019.04.004
23. Stoumpos, C.C. *et al.* (2013) Semiconducting tin and lead iodide perovskites with organic cations: phase transitions, high mobilities, and near-infrared photoluminescent properties. *Inorg. Chem.* 52, 9019–9038
24. Liu, C. *et al.* (2018) All-inorganic $CsPbI_2Br$ perovskite solar cells with high efficiency exceeding 13%. *J. Am. Chem. Soc.* 140, 3825–3828
25. Lin, J. *et al.* (2018) Thermochromic halide perovskite solar cells. *Nat. Mater.* 17, 261–267
26. Amat, A. *et al.* (2014) Cation-induced band-gap tuning in organohalide perovskites: interplay of spin-orbit coupling and octahedra tilting. *Nano Lett.* 14, 3608–3616
27. Ghosh, D. *et al.* (2017) Good vibrations: locking of octahedral tilting in mixed-cation iodide perovskites for solar cells. *ACS Energy Lett.* 2, 2424–2429
28. Zheng, X. *et al.* (2016) Improved phase stability of formamidinium lead triiodide perovskite by strain relaxation. *ACS Energy Lett.* 1, 1014–1020
29. Syzgantseva, O.A. *et al.* (2017) Stabilization of the perovskite phase of formamidinium lead triiodide by methylammonium, Cs, and/or Rb doping. *J. Phys. Chem. Lett.* 8, 1191–1196
30. Yi, C. *et al.* (2016) Entropic stabilization of mixed A-cation ABX_3 metal halide perovskites for high performance perovskite solar cells. *Energy Environ. Sci.* 9, 656–662
31. Lee, J. *et al.* (2015) Formamidinium and cesium hybridization for photo- and moisture-stable perovskite solar cell. *Adv. Energy Mater.* 5, 1501310

32. Shi, T. *et al.* (2014) Predictions for p-type $CH_3NH_3PbI_3$ perovskites. *J. Phys. Chem. C* 118, 25350–25354
33. Abdelhady, A.L. *et al.* (2016) Heterovalent dopant incorporation for bandgap and type engineering of perovskite crystals. *J. Phys. Chem. Lett.* 7, 295–301
34. Mitzi, D.B. (2000) Organic–inorganic perovskites containing trivalent metal halide layers: the templating influence of the organic cation layer. *Inorg. Chem.* 39, 6107–6113
35. Nayak, P.K. *et al.* (2018) Impact of Bi^{3+} heterovalent doping in organic–inorganic metal halide perovskite crystals. *J. Am. Chem. Soc.* 140, 574–577
36. Zhao, J. *et al.* (2017) Strained hybrid perovskite thin films and their impact on the intrinsic stability of perovskite solar cells. *Sci. Adv.* 3, eaao5616
37. Wenger, B. *et al.* (2017) Consolidation of the optoelectronic properties of $CH_3NH_3PbBr_3$ perovskite single crystals. *Nat. Commun.* 8
38. Parobek, D. *et al.* (2016) Exciton-to-dopant energy transfer in Mn-doped cesium lead halide perovskite nanocrystals. *Nano Lett.* 16, 7376–7380
39. Pan, G. *et al.* (2017) *Doping lanthanide into perovskite nanocrystals: highly improved and expanded optical properties*. 17 pp. 8005–8011
40. Yao, J. *et al.* (2018) Ce^{3+}-doping to modulate photoluminescence kinetics for efficient $CsPbBr_3$ nanocrystals based light-emitting diodes. *J. Am. Chem. Soc.* 140, 3626–3634
41. Wang, F. (2011) Tuning upconversion through energy migration in core–shell nanoparticles. *Nat. Mater.* 10, 968–973
42. Zhou, B. *et al.* (2016) Constructing interfacial energy transfer for photon up- and down- conversion from lanthanides in a core–shell nanostructure. *Angew. Chem. Int. Ed. Engl.* 55, 12356–12360
43. An, Y. *et al.* (2013) Highly efficient infrared quantum cutting in Tb^{3+}–Yb^{3+} codoped silicon oxynitride for solar cell applications. *Adv. Opt. Mater.* 1, 855–862
44. Berner, R.A. (1975) The role of magnesium in the crystal growth of calcite and aragonite from seawater. *Geochim. Cosmochim. Acta* 39, 489–504
45. Kubota, N. and Mullin, J.W. (1995) A kinetic model for crystal growth from aqueous solution in the presence of impurity. *J. Cryst. Growth* 152, 203–208
46. Sangwal, K. (1998) Growth kinetics and surface morphology of crystals grown from solutions: recent observations and their interpretations. *Prog. Cryst. Growth Charact. Mater.* 36, 163–248
47. Moore, D.T. *et al.* (2015) Crystallization kinetics of organic–inorganic trihalide perovskites and the role of the lead anion in crystal growth. *J. Am. Chem. Soc.* 137, 2350–2358
48. Xie, L.Q. *et al.* (2017) Understanding the cubic phase stabilization and crystallization kinetics in mixed cations and halides perovskite single crystals. *J. Am. Chem. Soc.* 139, 3320–3323
49. Wang, J.T.W. *et al.* (2016) Efficient perovskite solar cells by metal ion doping. *Energy Environ. Sci.* 9, 2892–2901
50. Zhang, J. *et al.* (2016) N-type doping and energy states tuning in $CH_3NH_3Pb_{1-x}Sb_{2x/3}I_3$ perovskite solar cells. *ACS Energy Lett.* 1, 535–541
51. Hu, Y. *et al.* (2017) Bismuth incorporation stabilized α-$CsPbI_3$ for fully inorganic perovskite solar cells. *ACS Energy Lett.* 2, 2219–2227
52. Hu, Y. *et al.* (2017) Enhancing moisture-tolerance and photovoltaic performances of $FAPbI_3$ by bismuth incorporation. *J. Mater. Chem. A* 5, 25258–25265
53. Wang, Z. *et al.* (2016) High efficiency Pb–In binary metal perovskite solar cells. *Adv. Mater.* 28, 6695–6703
54. Jena, A.K. *et al.* (2018) Stabilization of α-$CsPbI_3$ in ambient room temperature conditions by incorporating Eu into $CsPbI_3$. *Chem. Mater.* 30, 6668–6674
55. Xiang, W. *et al.* (2018) Europium-doped $CsPbI_2Br$ for stable and highly efficient inorganic perovskite solar cells. *Joule* 3, P205–P214
56. Wang, L. *et al.* (2019) A Eu^{3+}–Eu^{2+} ion redox shuttle imparts operational durability to Pb–I perovskite solar cells. *Science* 363, 265–270
57. Bi, C. *et al.* (2017) Spontaneous passivation of hybrid perovskite by sodium ions from glass substrates: mysterious enhancement of device efficiency revealed. *ACS Energy Lett.* 2, 1400–1406
58. Abdi-Jalebi, M. *et al.* (2018) Maximizing and stabilizing luminescence from halide perovskites with potassium passivation. *Nature* 555, 497–501
59. Abdi-Jalebi, M. *et al.* (2018) Dedoping of lead halide perovskites incorporating monovalent cations. *ACS Nano* 12, 7301–7311
60. Yang, Y. *et al.* (2018) Effect of doping of NaI monovalent cation halide on the structural, morphological, optical and optoelectronic properties of $MAPbI_3$ perovskite. *J. Mater. Sci. Mater. Electron.* 29, 205–210
61. Li, Y. *et al.* (2018) Lattice modulation of alkali metal cations doped $Cs_{1-x}R_xPbBr_3$ halides for inorganic perovskite solar cells. *Solar RRL* 2, 1800164
62. Zhao, W. *et al.* (2018) Alkali metal doping for improved $CH_3NH_3PbI_3$ perovskite solar cells. *Adv. Sci. (Weinh.)* 5, 1700131
63. Boopathi, K.M. *et al.* (2016) Synergistic improvements in stability and performance of lead iodide perovskite solar cells incorporating salt additives. *J. Mater. Chem. A* 4, 1591–1597
64. Son, D.Y. *et al.* (2018) Universal approach toward hysteresis-free perovskite solar cell via defect engineering. *J. Am. Chem. Soc.* 140, 1358–1364
65. Kubicki, D.J. *et al.* (2017) Phase segregation in Cs-, Rb- and K-doped mixed-cation $(MA)_x(FA)_{1-x}PbI_3$ hybrid perovskites from solid-state NMR. *J. Am. Chem. Soc.* 139, 14173–14180
66. Pazoki, M. *et al.* (2016) Effect of metal cation replacement on the electronic structure of metalorganic halide perovskites: replacement of lead with alkaline-earth metals. *Phys. Rev. B* 93, 144105
67. Frolova, L.A. *et al.* (2016) Exploring the effects of the Pb^{2+} Substitution in $MAPbI_3$ on the photovoltaic performance of the hybrid perovskite solar cells. *J. Phys. Chem. Lett.* 7, 4353–4357
68. Zhang, M. *et al.* (2017) High-efficiency rubidium-incorporated perovskite solar cells by gas quenching. *ACS Energy Lett.* 2, 438–444
69. Bai, X. *et al.* (2018) Effect of Rb doping on modulating grain shape and semiconductor properties of $MAPbI_3$ perovskite layer. *Mater. Lett.* 211, 328–330
70. Stoumpos, C.C. *et al.* (2015) Hybrid germanium iodide perovskite semiconductors: active lone pairs, structural distortions, direct and indirect energy gaps, and strong nonlinear optical properties. *J. Am. Chem. Soc.* 137, 6804–6819
71. Wang, K. *et al.* (2015) Lead replacement in $CH_3NH_3PbI_3$ perovskites. *Adv. Electron. Mater.* 1, 1500089
72. Kopacic, I. *et al.* (2018) Enhanced performance of germanium halide perovskite solar cells through compositional engineering. *ACS Appl. Energy Mater.* 1, 343–347
73. Ito, N. *et al.* (2018) Mixed Sn–Ge perovskite for enhanced perovskite solar cell performance in air. *J. Phys. Chem. Lett.* 9, 1682–1688
74. Yang, F. *et al.* (2018) All-inorganic $CsPb_{1-x}Ge_xI_2Br$ perovskite with enhanced phase stability and photovoltaic performance. *Angew. Chem. Int. Ed. Engl.* 57, 12745–12749
75. Klug, M.T. *et al.* (2017) Tailoring metal halide perovskites through metal substitution: influence on photovoltaic and material properties. *Energy Environ. Sci.* 10, 236–246
76. Almutawah, Z.S. *et al.* (2018) Enhanced grain size and crystallinity in $CH_3NH_3PbI_3$ perovskite films by metal additives to the single-step solution fabrication process. *Energy Mater. Technol.* 3, 3237–3242
77. Zhou, L. *et al.* (2017) Investigation of Fe^{2+}-incorporating organic–inorganic hybrid perovskites from first principles and experiments. *RSC Adv.* 7, 54586–54593
78. Saidaminov, M.I. *et al.* (2018) Suppression of atomic vacancies via incorporation of isovalent small ions to increase the stability of halide perovskite solar cells in ambient air. *Nat. Energy* 3, 648–654
79. Dunlap-Shohl, W.A. *et al.* (2016) Effects of Cd diffusion and doping in high-performance perovskite solar cells using CdS as electron transport layer. *J. Phys. Chem. C* 120, 16437–16445

80. Navas, J. *et al.* (2015) New insights into organic–inorganic hybrid perovskite $CH_3NH_3PbI_3$ nanoparticles. An experimental and theoretical study of doping in Pb^{2+} sites with Sn^{2+}, Sr^{2+}, Cd^{2+} and Ca^{2+}. *Nanoscale* 7, 6216–6229
81. Lu, Y. *et al.* (2017) Effective calcium doping at the B-site of $BaFeO_{3-\delta}$ perovskite: towards low-cost and high-performance oxygen permeation membranes. *J. Mater. Chem. A* 5, 7999–8009
82. Chan, S. *et al.* (2017) Enhancing perovskite solar cell performance and stability by doping barium in methylammonium lead halide. *J. Mater. Chem. A* 5, 18044–18052
83. Chen, C. *et al.* (2018) CaI_2: a more effective passivator of perovskite films than PbI_2 for high efficiency and long-term stability of perovskite solar cells. *J. Mater. Chem. A* 6, 7903–7912
84. Pérez-del-Rey, D. *et al.* (2016) Strontium insertion in methylammonium lead iodide: long charge carrier lifetime and high fill-factor solar cells. *Adv. Mater.* 28, 9839–9845
85. Wu, M.C. *et al.* (2018) The effect of strontium and barium doping on perovskite-structured energy materials for photovoltaic applications. *Appl. Surf. Sci.* 429, 9–15
86. Yao, E.P. *et al.* (2017) Efficient planar perovskite solar cells using halide Sr-substituted Pb perovskite. *Nano Energy* 36, 213–222
87. Wang, P. *et al.* (2018) Synthesis and characterization of Mn-doped $CsPb(Cl/Br)_3$ perovskite nanocrystals with controllable dual-color emission. *RSC Adv.* 8, 1940–1947
88. Liu, H. *et al.* (2017) $CsPb^xMn_{1-x}Cl_3$ perovskite quantum dots with high Mn substitution ratio. *ACS Nano* 11, 2239–2247
89. Van der Stam, W. *et al.* (2017) Highly emissive divalent-ion-doped colloidal $CsPb_{1-x}M_xBr_3$ perovskite nanocrystals through cation exchange. *J. Am. Chem. Soc.* 139, 4087–4097
90. Bai, D. *et al.* (2018) Interstitial Mn^{2+}-driven high-aspect-ratio grain growth for low-trap-density microcrystalline films for record efficiency $CsPbI_2Br$ solar cells. *ACS Energy Lett.* 3, 970–978
91. Chang, J. *et al.* (2016) Enhancing the photovoltaic performance of planar heterojunction perovskite solar cells by doping the perovskite layer with alkali metal ions. *J. Mater. Chem. A* 4, 16546–16552
92. Zhang, H. *et al.* (2017) $SrCl_2$ derived perovskite facilitating a high efficiency of 16% in hole-conductor-free fully printable mesoscopic perovskite solar cells. *Adv. Mater.* 29, 201606608
93. Turren-Cruz, S-H. *et al.* (2018) Enhanced charge carrier mobility and lifetime suppress hysteresis and improve efficiency in planar perovskite solar cells. *Energy Environ. Sci.* 11, 78–86
94. Kieslich, G. *et al.* (2014) Solid-state principles applied to organic–inorganic perovskites: new tricks for an old dog. *Chem. Sci.* 5, 4712–4715
95. Li, C. *et al.* (2004) Formability of ABO_3 perovskites. *J. Alloys Compd.* 372, 40–48
96. Li, C. *et al.* (2008) Formability of ABX_3 (X = F, Cl, Br, I) halide perovskites. *Acta Crystallogr B* 64, 702–707
97. Sun, Q. and Yin, W. (2017) Thermodynamic stability trend of cubic perovskites. *J. Am. Chem. Soc.* 139, 14905–14908
98. Brandt, R.E. *et al.* (2015) Identifying defect-tolerant semiconductors with high minority-carrier lifetimes: beyond hybrid lead halide perovskites. *MRS Commun.* 5, 265–275
99. Payne, D.J. *et al.* (2006) Electronic origins of structural distortions in post-transition metal oxides: experimental and theoretical evidence for a revision of the lone pair model. *Phys. Rev. Lett.* 96, 157403
100. Brivio, F. *et al.* (2014) Relativistic quasiparticle self-consistent electronic structure of hybrid halide perovskite photovoltaic absorbers. *Phys. Rev. B* 89, 155204
101. Chang, J. *et al.* (2017) New insights into the electronic structures and optical properties in the orthorhombic perovskite $MAPbI_3$: a mixture of Pb and Ge/Sn. *New J. Chem.* 41, 11413–11421
102. Harikesh, P.C. *et al.* (2018) Doping and switchable photovoltaic effect in lead-free perovskites enabled by metal cation transmutation. *Adv. Mater.* 30, 1802080
103. Wang, Q. *et al.* (2014) Qualifying composition dependent p and n self-doping in $CH_3NH_3PbI_3$. *Appl. Phys. Lett.* 105, 163508
104. Yin, W. *et al.* (2014) Unusual defect physics in $CH_3NH_3PbI_3$ perovskite solar cell absorber. *Appl. Phys. Lett.* 104, 063903